The International Journal of Advanced Manufacturing Technology (2023) 125:73–89
https://doi.org/10.1007/s00170-022-10631-3

ORIGINAL ARTICLE

Theoretical and numerical investigation of micro-textures fabrication by ultrasonic surface rolling process

Ying Meng[1] · Jianxin Deng[1] · Ran Wang[1] · Qinghao Sun[1] · Zhihui Zhang[1]

Received: 18 July 2022 / Accepted: 4 December 2022 / Published online: 20 December 2022

Abstract

Surface texturing is a potential approach to achieving excellent surface performance. To realize high precision and efficiency in micro-texturing fabrication, a surface texturing method utilizing an ultrasonic surface rolling process is proposed. Firstly, the feasibility and geometric controllability of micro-texture preparation using ultrasonic surface rolling process are analyzed. Then, a contact theory model of ultrasonic rolling texturing process is established, which can describe the geometric relationship of the micro-texturing generation region. Based on the elastic–plastic theory, simulations of single-pass and multi-pass ultrasonic rolling texturing processes are developed to elucidate the formation and strengthening mechanism of micro-textures, and further characterize the effects of ultrasonic rolling machining parameters on micro-textures. A series of validation tests of ultrasonic rolling texturing are implemented on AISI 5140 steel. Simulation and experimental results show that the ultrasonic surface rolling process can fabricate micro-groove arrays with the periodic distribution. The validity of the theoretical and finite element models is confirmed by the comparison results. It is demonstrated that the ultrasonic rolling texturing process is a feasible and efficient way to fabricate controllable micro-textures.

Keywords Ultrasonic surface rolling process · Surface texture · Fabrication mechanism · Theoretical analysis · Finite element model

1 Introduction

Textures originate from the topological patterns formed on natural surfaces that have excellent properties such as friction reduction, drag reduction, lubrication, self-cleaning, and anti-fouling [1, 2]. Currently, textures have developed into functionalized structures with specific distribution patterns and geometric shapes. The specific role played by surface textures opens up more possibilities for practical applications of non-smooth surfaces. In particular, attention has increased to improving mechanical and tribological behavior by introducing surface textures in recent decades [3, 4]. Textured surfaces are known to be effective in reducing actual contact area, trapping wear debris, mitigating wear, acting as a reservoir, preventing lubricant starvation, and producing hydrodynamic effects [5–7]. Surface texturing technology has a promising application in mechanical manufacturing, medicine, micro-nano electromechanical systems (MEMS/NEMS), and new energy [8–10].

To meet the requirements for surface properties responding to different fields, various techniques for fabricating surface textures have been developed, including laser surface texturing (LST), focused ion beam (FIB), chemical etching, lithography, electro discharge machining (EDM), and micro-cutting. Salguero et al. [4] created multiple texture types by varying the energy density and scanning speed of the laser pulse. Kawasegi et al. [11] successfully produce textures on the rake face of the tool utilizing FIB and found that the cutting performance of the tool was enhanced. Shimizu et al. [12] suggested a new method for surface texturing by vibration-assisted micro-cutting using a diamond head that vibrated with a certain amplitude in the depth direction. In addition, different texturing strategies can be utilized in conjugation with one another, such as ultrasonic-assisted micro-grinding and laser peen texturing (LPT). Li et al. [13] fabricated micro-textures with different densities on copper surfaces using LPT technology and the result showed that LPT is a feasible technique to produce controllable

✉ Jianxin Deng
jxdeng@sdu.edu.cn

[1] Key Laboratory of High Efficiency and Clean Mechanical Manufacture of MOE, School of Mechanical Engineering, Shandong University, Jinan 250061, China

micro-textures. Although surface texturing has been applied to many manufacturing processes, its complex mechanism, expensive equipment, low accuracy, and limited output have become constraints for industrial services. Thus, under such circumstances, seeking low-cost, high-efficiency, and high-precision texturing methods is an urgent need in the field of texture processing.

Ultrasonic surface rolling process (USRP) is an emerging modification technique that combines deep rolling and ultrasonic impact machining. It involves the surface severe plastic deformation (S^2PD) methodology and results in enhanced surface mechanical performance. During the rolling process, ultrasonic vibrations act simultaneously on the rolling head to continuously impact the surface being machined. USRP is considered to be an outstanding technology for increasing the residual compressive stress and reducing the roughness of the material surface [14]. Karademir et al. [15] investigated the mechanical properties and microstructure of steel after ultrasonic nanocrystal surface modification and found that the material achieved a dual strength-ductility improvement through the modified gradient structure. Wang et al. [16] proved that the surface roughness of X80 pipeline steel decreased to 0.2 μm after USRP, which was 15% of that of the untreated specimen, and that the residual stress remarkably changed from tensile to compressive. Besides, in the field of surface texturing, Kheradmandfard et al. [17] unexpectedly found that ultrasonic nanocrystal surface modification led to the formation of micro-patterns on the titanium alloy surface, which was induced by the treatment tracks and would be beneficial for high bioactivity and bone regeneration performance of the implants.

To take full advantage of texturing, many studies have explored the significance of texturing parameter optimization for performance applications and found that inappropriate parameters may deteriorate material properties. The design of key parameters of textures includes shapes, distribution positions, geometric parameters (depth, width, and density), and combination form. Currently, the design of texture parameters has not formed a unified system. Design of experiments is the straightforward and commonly used method for establishing relationships between texture parameters and surface properties. However, it needs the costs most, including manufacturing, material, and equipment costs. Analytical calculations and numerical simulations can improve the texture fabrication process with small inputs. Nevertheless, few studies on the preparation of textures using USRP are available.

In this study, we developed a new high-precision mechanical texturing method in which USRP was used to fabricate textured surfaces with periodically arranged micro-grooves. A systematic theoretical, numerical and experimental study was performed to understand the USRP texturing process and fabrication mechanism. Here, a particular effort was made to clarify the effect of USRP process parameters on the micro-texture geometry. The comparative analysis of the results verifies the feasibility of the USRP texturing process models.

2 Theoretical contact model of USRP texturing process

2.1 Feasibility analysis of micro-texture fabrication by USRP

USRP can cause significant elastic–plastic deformation of the material through continuous extrusion and periodic ultrasonic vibration, thereby affecting the surface integrity. Figure 1 shows the elastic–plastic contact process in the machined region during USRP based on the Hertzian contact theory. When the rolling head is deformed in contact with the machined surface, the plastic flow on the contact surface creates a concave micro-groove with an approximately arc-shaped cross-section, whose radius is related to the size of the contact arc of the rolling head. After the rolling head is removed, the cross-sectional radius of the concave micro-groove will increase and the depth will decrease slightly due to partial elastic recovery. The deformation state of the contact area is shown in Fig. 2, where the rolling head is in contact with the machined surface, forming a concave

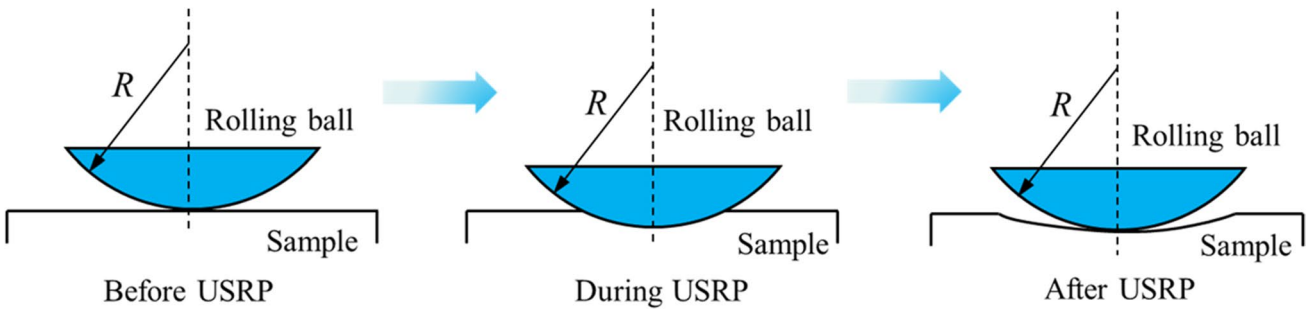

Fig. 1 The elastic–plastic deformation process in USRP

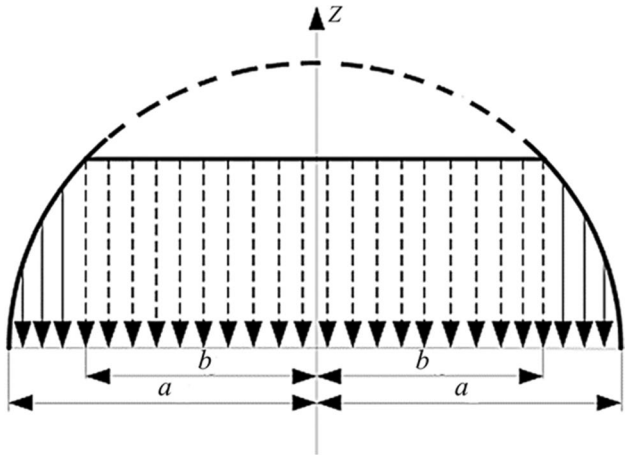

Fig. 2 The contact deformation state of the machined area

micro-groove, where a is the contact radius and b is the radial distance from the center to the elastic–plastic contact stress boundary point [18]. It can be found that the rest of the micro-groove formation area is in the elastic deformation stage, showing Hertzian contact stress distribution, and the contact stress gradually decreases from a maximum value to zero. The contact stress is uniformly distributed in the micro-groove formation area, where irreversible and complete plastic deformation occurs, providing feasibility for the preparation of micro-textures.

In addition to fabricating surface topologies, USRP enables the machined material surface to induce excellent mechanical properties such as high hardness and ideal residual compressive stress. In USRP, plastic deformation dominated by deformation strengthening leads to significant changes in the microstructure of the machined material surface, which is overall manifested by the formation of a gradient modified layer structure varying along the machining depth direction, as shown in Fig. 3. The grain refinement effect of the surface is progressively weakened along the machining depth direction. The modified layers are mainly presented as the fine grain modified layer (I), subsurface modified layer (II), intermediate deformation layer (III), and matrix layer (IV) in order. The degree of grain refinement, the degree of plastic deformation, and the depth of the gradient modified layer are closely related to the USRP processing parameters. Based on the above analysis, the substrate surface can form a micro-textured three-dimensional structure with the strengthening layer under in-situ USRP processing.

Compared to some common micro-texturing fabrication methods such as laser surface processing (LSP), electric spark machining (EDM), shot peening (SP), and grinding, the unique features of the USRP texturing process are:

(1) USRP equipment can be assembled with machining systems, such as machine tools and machining centers. Good matching with the machining system ensures real-time control of the machining process and guarantees controlled adjustment of the machining trajectory. Especially with the development of CNC machines, USRP can be better adapted to flexible and variable machining requirements, thus enabling efficient surface micro-texturing.
(2) The feed speed of the machining system is controlled and constant. Once the output amplitude and frequency of the rolling ball are set, the dynamic impact force is also controlled and constant. Static pressure is determined by air pressure. Consequently, the output energy of the rolling ball is uniform and stable at all times during the USRP machining process, which ensures consistent and controllable machining of micro-texture dimensions.
(3) The transition between adjacent ultrasonic vibration impact regions is achieved by close rolling of the working head, which largely eliminates the overlap between indentations, thus guaranteeing the machining accuracy of the micro-texture. In addition, the combined effect of ultrasonic vibration and rolling can lead to uniform stress and increased deformation. Accordingly, the high-precision micro-textures with enhanced properties are obtained.
(4) No obvious fault between the surface reinforced layer and the substrate structure so that the reciprocal machining cannot cause damage to the material sur-

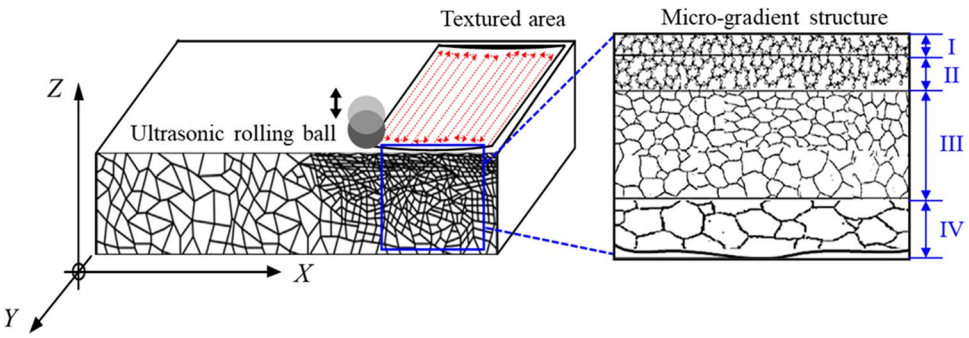

Fig. 3 Gradient micro-structure of the modified layer after USRP

face. This ensures the surface quality and machining accuracy of the micro-textures on the one hand and broadens the machinable range of the micro-texture dimensions on the other hand.

2.2 Geometric controllability analysis of USRP texturing process

USRP is a process in which static pressure and dynamic impact force act together. The static pressure is applied continuously and its value is uniquely determined by the air pressure. The dynamic impact force propagates as a resonant ultrasonic impact, and the magnitude of which is controlled by the parameters of the ultrasonic generator, which mainly include the frequency, amplitude, and load of the ultrasonic vibration. For the ultrasonic generator with a fixed type, the frequency is a defined value. The ultrasonic amplitude can be varied within a certain range by adjusting the current and voltage of the ultrasonic generator. The dynamic impact force of the resonant wave generally varies as a sine wave function, and the periodically varying sine wave is loaded through a Fourier function. The specific function form is:

$$f(t) = A_0 + \sum_{n=1}^{\infty} \left(a_n \cos n\omega t + b_n \sin n\omega t\right) \tag{1}$$

where A_0 is the load and is a constant term, a_n and b_n are the amplitudes of the harmonics, n is the number of harmonics, and ω is the angular frequency of the ultrasonic wave. The static pressure in the USRP can be applied separately as a concentrated force or defined in A_0.

In USRP machining, the resonant wave varies as a sinusoidal function, i.e., $a_n = 0$ and $b_n = 1$, and its variation curve is shown in Fig. 4. It can be found that the x-coordinate is mainly determined by the ultrasonic vibration frequency, while the y-coordinate is decided by the load and ultrasonic amplitude. In other words, the magnitude of the dynamic impact force during USRP machining is adjustable, and its value changes periodically with the change of frequency, amplitude, and load. As emphasized in Fig. 5, the static pressure and dynamic impact force applied to the machined surface during USRP can be available determined by parameter adjustments.

The USRP texturing process can be simplified as the contact between the ball and the plane. According to the contact mechanics theory, the contact area between the rolling ball and the surface is in the elastic–plastic deformation stage during the USRP texturing process. The elastic–plastic behavior of the machined region complicates the contact problem in the USRP texturing process. In addition to the non-linearity of contact mechanics, the non-linearity of geometric deformation is also included, which is beyond the scope of the application of Hertzian elastic contact theory. Therefore, the contact deformation behavior during USRP texturing must be analyzed from the perspective of elastic–plastic contact.

In the USRP texturing process, the total rolling force is a superposition of the static pressure and the ultrasonic vibration impact force. In addition to the formation of micro-texture related to the continuously applied static pressure, the changes in the machining trajectory of the rolling ball under the action of ultrasonic vibration impact also have an impact on the formation of micro-texture. Figure 6 shows the contact process under static pressure and ultrasonic vibration impact during the single-pass texturing process, where L is the single-pass machining length; S is the center distance between two adjacent passes, i.e., the machining step; V_f is the feed speed along the X-axis direction; a is the actual contact radius; t is the machining time; h is the micro-texture depth; R is the ultrasonic rolling ball radius. As shown in

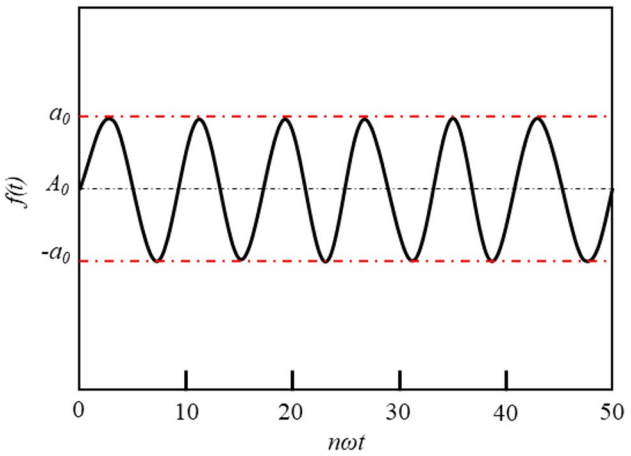

Fig. 4 The sine function curve of the resonant wave

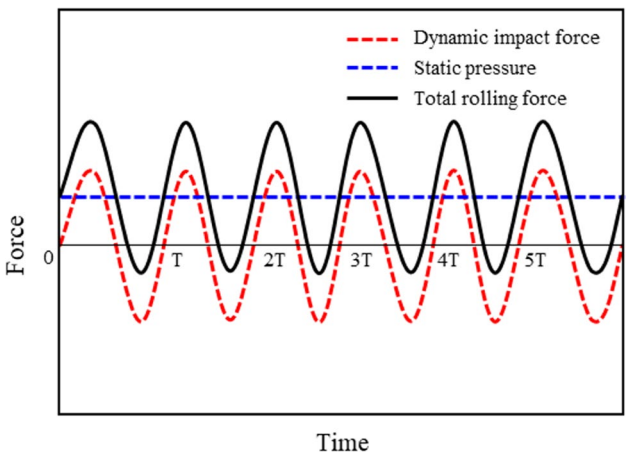

Fig. 5 The variation of rolling force during USRP machining

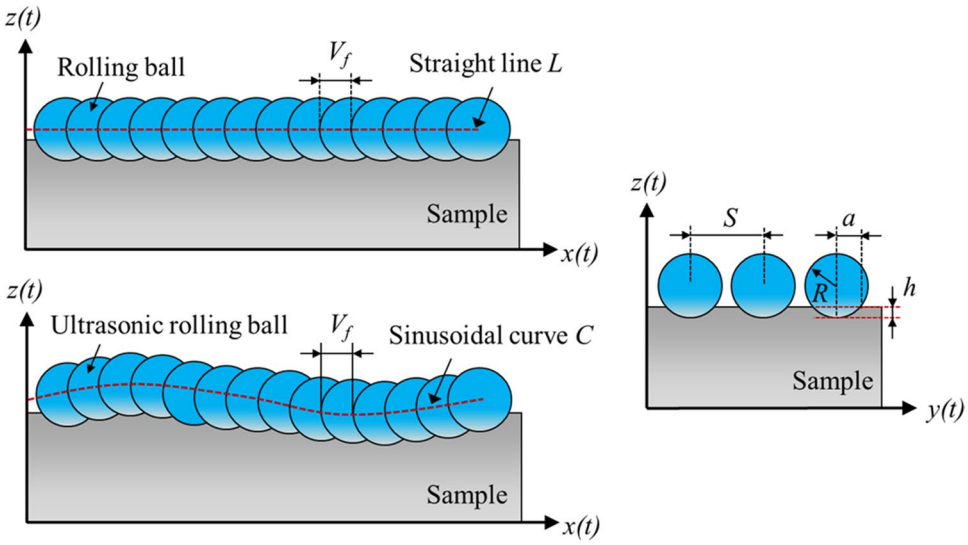

Fig. 6 Trajectory variation of the rolling ball under static pressure and ultrasonic vibration impact

Fig. 6, during the single-pass texturing processing without the application of ultrasonic vibration impact, the feed trajectory of the rolling ball along the Z direction under the action of static pressure is a straight line L, and the surface area of the formed micro-groove is $A_0 = 2a \bullet L = 2aV_f t$. After the introduction of ultrasonic vibration impact, the feed machining trajectory of the ultrasonic rolling ball along the Z direction is a sinusoidal curve C, whose length can be expressed as follows:

$$C = \int \sqrt{1 + z''(t)} \tag{2}$$

Thus, the actual surface area A_{USRP} of the micro-texture is:

$$A_{\mathrm{USRP}} = 2a \bullet C = 2a \int \sqrt{1 + z''(t)} \tag{3}$$

For a steel material with a Poisson's coefficient of 0.3, when initial yielding occurs, the contact radius a can be expressed as follows [19]:

$$a = 2.306 \frac{\sigma_y}{E^*} R \tag{4}$$

where σ_y is the yield strength of the machined material, E^* is the reduced modulus, $E^* = E_1/(1\text{-}v_1) + E_2/(1\text{-}v_2)$. E_1 and E_2 are the elasticity modulus of the rolling ball and the machined material, respectively. v_1 and v_2 are the Poisson's coefficients of the rolling ball and the machined material, respectively.

Finally, the A_{USRP} can be described as follows:

$$A_{\mathrm{USRP}} = 4.612 \frac{\sigma_y}{E^*} R \int_0^{\frac{L}{V_f}} \sqrt{1 + (2\pi\omega A)^2 cos^2(2\pi\omega t)} dt \tag{5}$$

where A is the amplitude of the ultrasonic vibration impact force.

The machined dimensions of the micro-texture are influenced by the geometric relationship of the machined contact region. According to the contact theory, the shape of the contact region between the rolling ball and the machined surface is approximately spherical, as illustrated in Fig. 7, where F_N is the total force exerted on the rolling ball; N is the contact pressure; f is the friction force; θ is the angle between the contact surface and the Z-axis; φ is the angle between the projection of the contact surface in the X–Y plane and the Z-axis.

To acquire the pressure N operating on the contact area, the contact area is partitioned into discrete equidistant cells. Assuming that the pressure N_i is approximately constant $d\overrightarrow{N}$ in the ith interval, the total contact pressure N can then be obtained by integrating over the contact area as follows:

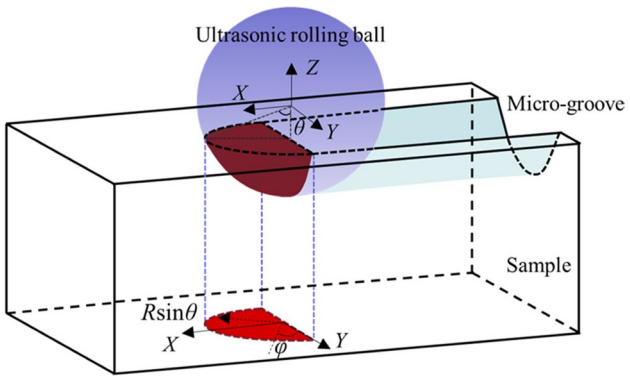

Fig. 7 Contact geometrical model during USRP texturing process

$$\overrightarrow{N} = \iint \overrightarrow{dN} \tag{6}$$

$$dN = PdA = P \bullet (Rd\theta) \bullet (Rsin\theta d\varphi) = P \bullet R^2 \sin\theta d\theta d\varphi \tag{7}$$

where P is the average contact stress. The interval contact area dA is calculated based on the model in Fig. 8. The individual components of N decomposed along the X, Y, and Z directions are expressed as follows:

$$\overrightarrow{N} = \overrightarrow{N_x} + \overrightarrow{N_y} + \overrightarrow{N_z} \tag{8}$$

$$\overrightarrow{N_x} = -\iint dN sin\theta sin\varphi = -PR^2 \int_0^{\alpha} sin^2\theta d\theta \int_0^{\pi} sin\varphi d\varphi \tag{9}$$

$$\overrightarrow{N_y} = 0 \tag{10}$$

$$\overrightarrow{N_z} = -\iint dN cos\theta = -PR^2 \int_0^{\alpha} sin\theta cos\theta d\theta \int_0^{\pi} d\varphi \tag{11}$$

According to Coulomb's law, the frictional components along the X, Y, and Z axes are calculated as follows:

$$\vec{f} = \iint \overrightarrow{df} \tag{12}$$

$$\vec{f} = \vec{f_x} + \vec{f_y} + \vec{f_z} \tag{13}$$

$$\vec{f_x} = \mu\overrightarrow{N_y} = -\mu PR^2 \int_0^{\alpha} sin\theta cos\theta d\theta \int_0^{\pi} d\varphi \tag{14}$$

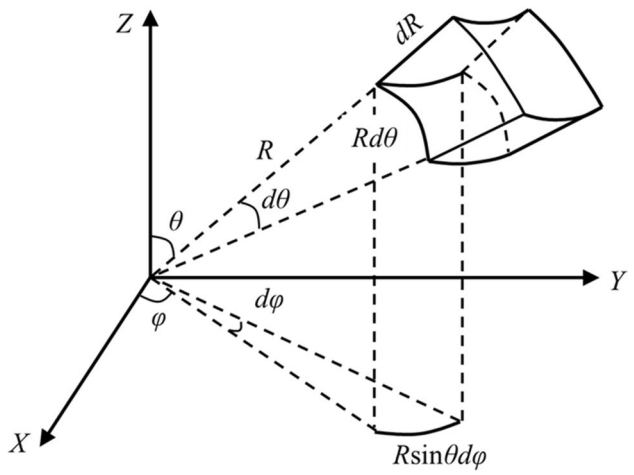

Fig. 8 Triple integral calculation model in the spherical coordinate system

$$\vec{f_y} = 0 \tag{15}$$

$$\vec{f_z} = \mu\overrightarrow{N_x} = -\mu PR^2 \int_0^{\alpha} sin^2\theta d\theta \int_0^{\pi} sin\varphi d\varphi \tag{16}$$

where the directions of $\overrightarrow{dN}$ and $\overrightarrow{df}$ are perpendicular to each other, and μ is the friction coefficient of the contact surface.

According to Newton's law, the forces acting on the ultrasonic rolling ball are balanced, so the resultant force along the Z-axis should be zero:

$$\overrightarrow{F_N} + \overrightarrow{N_z} + \vec{f_z} = 0 \tag{17}$$

Substituting Eqs. (11) and (16) into Eq. (17):

$$\begin{aligned} F_N &= \tfrac{1}{4}\pi R^2 P\left[(1 - cos2\alpha) - \tfrac{2}{\pi}\mu(2\alpha - sin2\alpha)\right] \\ &\approx \pi \mathrm{RPh}\left[1 - \mu\sqrt{\tfrac{h}{2R}}\right] \end{aligned} \tag{18}$$

Since the micro-texture depth h is much smaller than the rolling ball diameter $2R$, $h/2R$ is approximated as 0. The friction coefficient μ during USRP texturing process is very small and can be ignored. Furthermore, according to Tabor's theory [19], the average contact stress P can be approximately expressed as $2.8H$ (H is the material hardness) when the contact state of the machined region is in the fully plastic deformation stage. So, Eq. (18) can be approximately simplified as:

$$F_N = \pi \mathrm{RPh} = 2.8\pi \mathrm{RHh} \tag{19}$$

Then, the depth of micro-texture can be approximated as follows:

$$h = \frac{F_N}{2.8\pi RH} \tag{20}$$

As illustrated in Eq. (20), the depth of micro-texture fabricated by USRP is mainly related to the rolling force, the radius of the rolling ball, and the surface hardness of the material being machined. When the radius of the rolling ball is constant, the micro-texture depth processed by the single-pass USRP texturing is proportional to the rolling force. Zhao et al. [20] established the relationship between rolling force and rolling depth in rotary ultrasonic rolling through simulations and experimental studies and came to similar conclusions as in the present study. They found that the rolling depth increased linearly with the increase of rolling force without changing other process parameters. In addition, they also found that the influence of static pressure on rolling depth was much greater than that of dynamic impact force through the experimental results.

From Eqs. (5) and (20), it can be seen that in the single-pass USRP texturing process, the dimensional parameters

of the micro-texture are related to the properties of the material to be machined, rolling ball parameters, static pressure, feed speed, ultrasonic vibration frequency, and amplitude. It should be noted that in the preparation of periodically arranged micro-textures, multiple-passes ultrasonic rolling on the surface is required. At this time, the distance between adjacent passes is determined by the set step distance, which is directly related to the spacing of the micro-textures. Based on the above theoretical analysis, the dimensional parameters of micro-texture are closely related to the USRP machining parameters, and there is a certain mapping relationship between them. Therefore, it is feasible to prepare regular and controllable surface micro-textures by adjusting the USRP machining parameters.

3 Numerical analysis of the USRP texturing process

Numerical simulation is an important analytical method to study the machining mechanism and process parameters of advanced manufacturing technology [21–23]. Therefore, based on the elastic–plastic contact theory, the finite element model (FEM) is employed to study the machining mechanism of the USRP texturing process. The theoretical analytical model suggests that many parameters affect the USRP texturing effect, which can lead to a very large research effort. Hence, we selected the machining parameters that have obvious influence and are of more concern to the staff in the actual machining process for a preliminary discussion. Considering the high degree of freedom required for surface texturing, cemented carbide ball was selected as an ultrasonic rolling head. Next, based on the established FEM model of USRP texturing, the influence of static pressure, ultrasonic amplitude, feed speed, and step distance on the machining effect of the USRP texturing process were focused on.

3.1 Kinematic analysis of ultrasonic rolling ball

During the USRP texturing process, static pressure and ultrasonic vibration are applied to the rolling head along the direction of the machine spindle (Z direction), the machined sample is fixed to the worktable, and the rolling ball is fed in the X and Y direction relative to the sample being machined. Assuming that the machined sample is stationary, the motion of the rolling ball can be expressed as a compound motion in two directions: the feed motion along the machining direction and the ultrasonic vibration along the spindle direction. When the rolling ball is fed along the X direction to process the micro-groove, the equation of motion displacement at the center of the rolling ball can be expressed as:

$$\begin{cases} x(t) = v_f t \\ z(t) = A sin(2\pi\omega t) \end{cases} \tag{21}$$

Figure 9 shows the machining displacement trajectory of the rolling ball based on Eq. (21) at a feed speed v_f of 1000 mm/s, an ultrasonic amplitude A of 7 μm, and an ultrasonic vibration frequency ω of 28 kHz. It can be seen that the rolling ball moves in a periodic sinusoidal trajectory in the depth direction of the USRP texturing process. Nevertheless, during the actual USRP texturing process, the trajectory of the rolling ball is influenced by the static pressure in addition to the ultrasonic vibration impact, as represented in Fig. 5.

To explore the kinematics of the ultrasonic rolling ball during USRP texturing process, a single-point ultrasonic vibration impact model under the joint action of static pressure and dynamic impact force was established via ABAQUS 6.14 software. A sphere with a diameter of 8 mm is selected for the ultrasonic rolling head. The sample to be impacted is a plane. The stress–strain field during single-point vibration impact is symmetrical, so the impacted sample is set as a quarter-cube model with a side length and height of 14 mm and 10 mm, respectively. The impacted substrate is AISI 5140 steel and the rolling head is YG6 cemented carbide ball. The basic material parameters are presented in Table 1. The stiffness of YG6 is much greater than that of the AISI 5140 steel, so the rolling ball is set as a non-deformable analytic rigid body. The deformed steel substrate meshes with an eight-node linearly reduced integral element (C3D8R). The mesh in the contact area of the machined substrate is refined and gradually transitions to a coarser mesh towards the boundary. Considering the computational cost, the minimum cell size is 0.05 mm.

During USRP texturing processing, the rolling ball acts on the material surface with mechanical vibrations at ultrasonic frequencies, and the machined material surface produces severe deformation, resulting in a strain rate range of ~ 10^3 ~ 10^4, accompanied by significant work hardening and strain rate hardening phenomena. For the deformation at a high strain rate, Johnson and Cook designed the Hopkinson compression bar experiment and obtained the Johnson–Cook (JC) constitutive model considering the strain rate effect [24]. The expression is as follows:

$$\sigma = (\varepsilon, \dot{\varepsilon}, T) = (A + B\varepsilon^n)\left[1 + C\ln\left(\frac{\dot{\varepsilon}}{\dot{\varepsilon}_0}\right)\right]\left[1 - (T^*)^m\right] \tag{22}$$

where σ is the flow stress, ε is the strain, $\dot{\varepsilon}$ is the strain rate, A is the yield stress, B is the strain hardening modulus, n is the hardening index, C is the strain rate sensitivity coefficient, T^* is the temperature-dependent factor, and m is the thermal softening index.

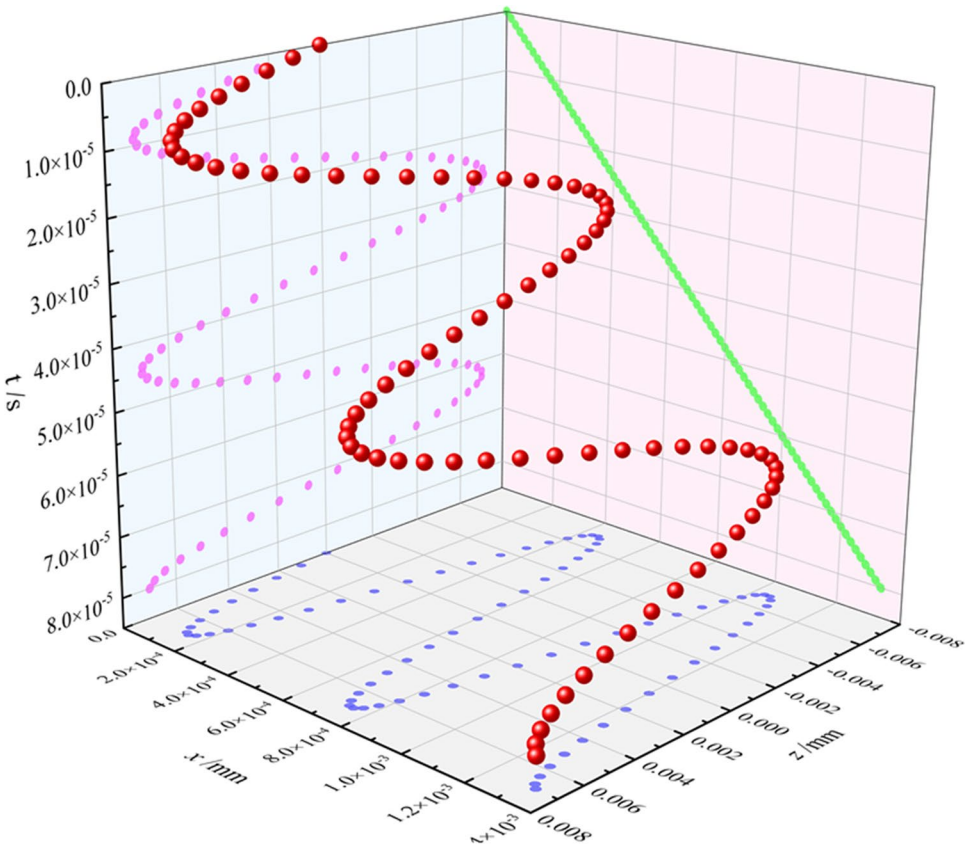

Fig. 9 Theoretical trajectory of rolling ball in the ultrasonic vibration impact model

Table 1 Material parameters

Parameters	AISI 5140 steel	YG6 cemented cabide
Density (kg/m^3)	7.85×10^3	15×10^3
Elastic modulus (GPa)	210	710
Poisson's coefficient	0.3	0.21

Table 2 The JC constitutive model parameters of AISI 5140 steel

A (MPa)	*B* (MPa)	*C*	*n*
850	563	0.134	0.234

The JC model is accurate for the description of plastic deformation of most metal materials. It has been widely used in numerical simulation research in areas such as cutting, stamping, and rolling due to its simple form and convenient calculation [25]. The USRP texturing process is performed at room temperature, where the machining temperature is much lower than the phase transition temperature of the base steel, so the parameters of the constitutive model related to the thermal effect are not explored. The remaining parameters of AISI 5140 steel are shown in Table 2 [26].

The initial loading conditions for the USRP texturing process are static pressure and dynamic impact force. The dynamic impact force, which varies periodically according to the sine function, is loaded by the Fourier function using the amplitude function of ABAQUS. The dynamic impact force is input according to the values measured by the piezoelectric sensing force test, as shown in Table 3. Both the static pressure and dynamic impact force are concentrated loads applied at the center of the rolling ball (reference point *RP*). A contact pair is set up between the rolling ball and the substrate surface using a penalty function contact algorithm with the Coulomb friction coefficient of 0.15. The bottom of the sample to be machined is constrained and symmetrical boundary conditions are imposed on the symmetry plane. The entire model contains 14,700 units.

Table 3 Dynamic impact force values corresponding to different static pressures and amplitudes

Static pressures/N	Amplitude/μm			
	5	7	9	11
300	67.5	85.5	110	130.5
450	70.5	92	117.5	136.5
600	76.5	100	123.5	155.5
900	85.5	118	137.5	176.5

Figure 10 shows the impact velocity V_2 (velocity along the machining depth direction) of the rolling ball versus time

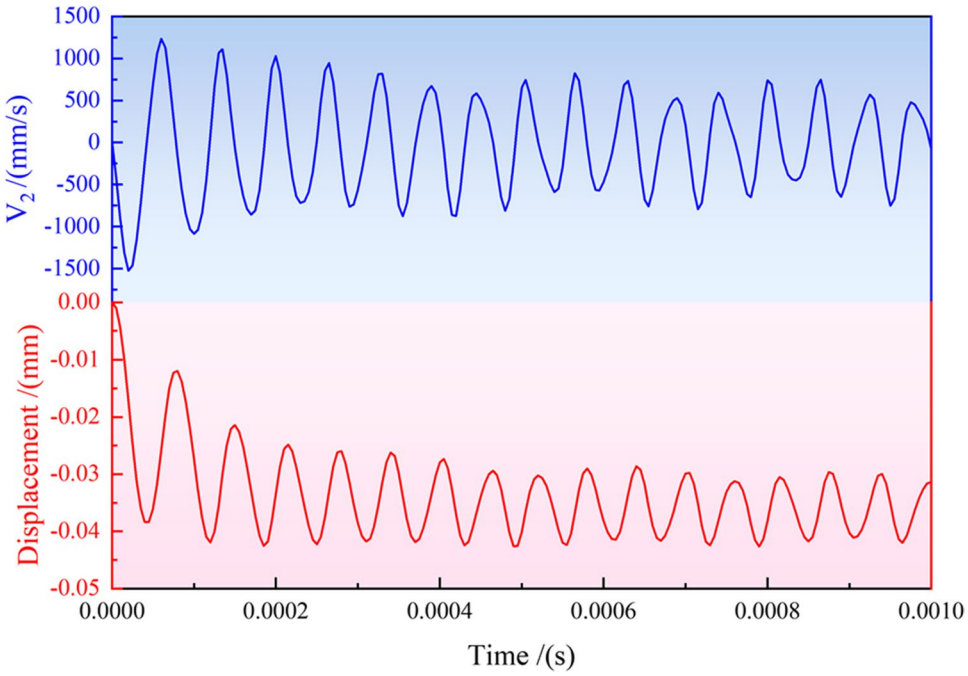

Fig. 10 Velocity and displacement curve of the ball along machining depth direction during the single-point ultrasonic vibration impact process

for 1 ms at an ultrasonic vibration frequency of 28 kHz, an amplitude of 7 μm, and a static pressure of 300 N. At the first impact, the V_2 is negative and has a large value owing to the combined effect of static pressure and dynamic impact force. The maximum value of V_2 is ~ 1500 mm/s, which indicates that the ball is always pressed against the sample surface. The velocity of subsequent impacts decreases with time. Such behavior is due to the increase of the static pressure at the first impact from 0 to 300 N, which corresponds to an instantaneous load in a very short time together with the dynamic impact force, thus affecting the ball velocity. In the subsequent impacts, the static pressure remains constant while the dynamic impact force dominates the motion state of the ball. The variation range of V_2 begins to decrease from the second impact and gradually stabilizes after five or six impacts. At the same time, the rebound velocity of the ball also reduces with the impact velocity. Figure 10 also displays the displacement variation D_2 (displacement along the machining depth direction) of the ball within 1 ms. It can be seen that the variation tendency of D_2 is similar to V_2. The downward displacement of the ball is greatest at the first impact, where the instantaneous change of static pressure plays a leading role. The fluctuation behavior of D_2 indicates that the machined material is in an alternate state of elastic–plastic deformation and rebound deformation. In subsequent impacts, the maximum impact depth gradually decreases. Similarly, after five or six impacts, the downward displacement tends to be stable, which indicates that irrecoverable plastic deformation occurs on the machined surface, that is, a micro-dimple topology is formed. Also, the continuous imposition of static pressure prevents the ball from returning to its initial position on the rebound, so the displacement is always negative. The static pressure has a more significant effect on the depth of the micro-dimple than the dynamic impact force. In general, different processing parameters may produce different impact velocities and displacements of the balls; however, the variation pattern between the two is basically unchanged.

3.2 Establishment of FEM model for USRP texturing process

To reveal the fabrication process and formation mechanism of USRP micro-texturing more accurately, the single-pass and multi-pass USRP texturing processes are simulated by ABAQUS. The machined sample is set as a cuboid model with the dimension of $15 \times 15 \times 5$ mm^3, which is consistent with the parameters of the subsequent tests. The substrate material is AISI 5140 steel and the plastic parameters are entered based on the JC model in Table 1. The ultrasonic rolling head is set up as a non-deformable analytical rigid body, which is a 6 mm diameter sphere. The material properties of the ultrasonic rolling ball and the machined substrate are the same as those described in the single-point ultrasonic vibration impact model. The contact in the machining area is set as surface-to-surface contact. The bottom of the machined substrate is fully constrained and the clamping area is symmetric with boundary constraints. To reduce the solution time and improve the calculation rate, the meshing of the contact machining region is refined by partitioning with a minimum element

size of 0.05 mm. The mesh is progressively transitioned to the non-processed areas in a 10:1 ratio under conditions where the stresses and strains in the machined region could be reasonably converged. The ultrasonic vibration frequency is 28 kHz, which is the same as the subsequent tests. A 15 mm long single-path ultrasonic rolling process is performed on the substrate surface.

The sequential simulation machining of multi-pass USRP texturing is realized by applying commands for the initial predefined field in ABAQUS. After completing a single-pass USRP texturing process, its result file is set to predefined fields as the initial state for the next texturing analysis pass. Then, the parameters of the analysis step are changed according to the texturing requirements. Finally, the result of the sequential superposition of the machining passes is the simulation result of USRP micro-textures in multi-pass treatment. The established FEM model of the USRP texturing process is shown in Fig. 11. The FEM model consists of 387,600 units.

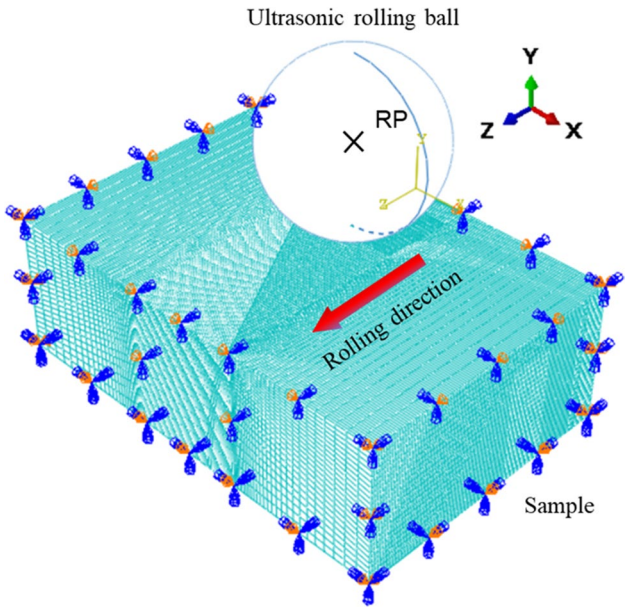

Fig. 11 FEM model of USRP texturing process

3.3 Predictive analysis based on the FEM model of USRP texturing process

The single-pass USRP texturing process is first simulated, and the effects of static pressure, feed speed, and amplitude on the dimension of the micro-textures are emphatically studied, as shown in Fig. 12. In the singular effect analysis, the remaining parameters are fixed at a static pressure of 300 N, an amplitude of 7 μm, and a feed speed of 1000 mm/min. As seen in Fig. 12, the single-pass ultrasonic rolling successfully fabricated a regular micro-groove topology on the steel substrate surface. Static pressure shows the most significant effect on the dimension of the micro-groove, followed by feed speed, with the least effect on amplitude. As the static pressure increases, both the depth and width of the micro-groove increase significantly, especially the depth. The depth of the micro-groove decreases with increasing feed speed, while the width of the micro-groove changes slightly. In contrast, the effect of amplitude on the dimensional profile of the micro-groove is not significant.

In practical applications, the surface micro-textures are distributed over a large area and arranged periodically. Therefore, based on the established FEM model, the multi-pass USRP texturing process is simulated. The effects of USRP parameters (air pressure, feed speed, step distance) on the strain, stress, and energy during the surface texturing process are emphatically studied. In order to visualize the surface topography variations of the micro-textures, the deformation scaling factor is set to 20 in the post-processing stage of the FEM model. Figure 13 shows the displacement simulation contour (U_2, along the machining depth direction) of the textured surface at a static pressure of 450 N, a feed speed of 1000 mm/min, an amplitude of 7 μm, a step distance of 200 μm, and 6 machining passes. The contour

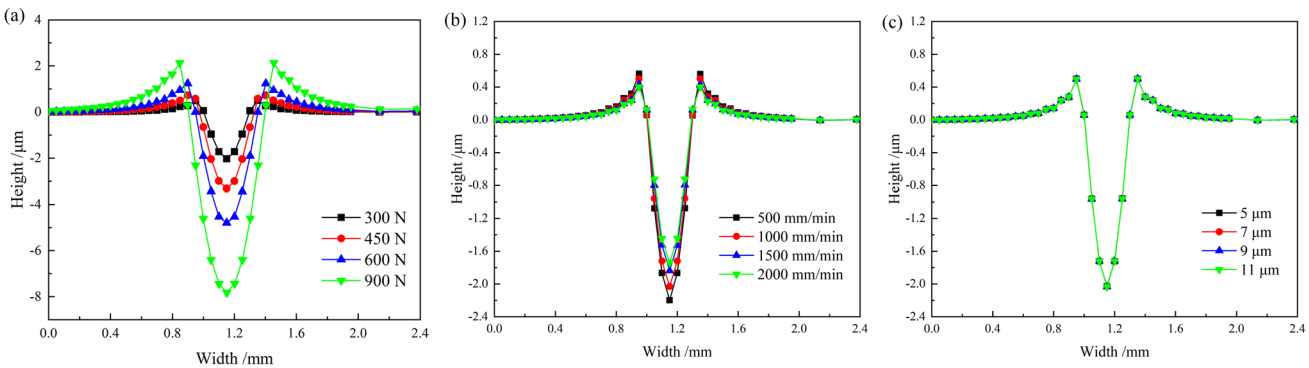

Fig. 12 Influence of parameters on micro-groove dimension in single-pass USRP texturing

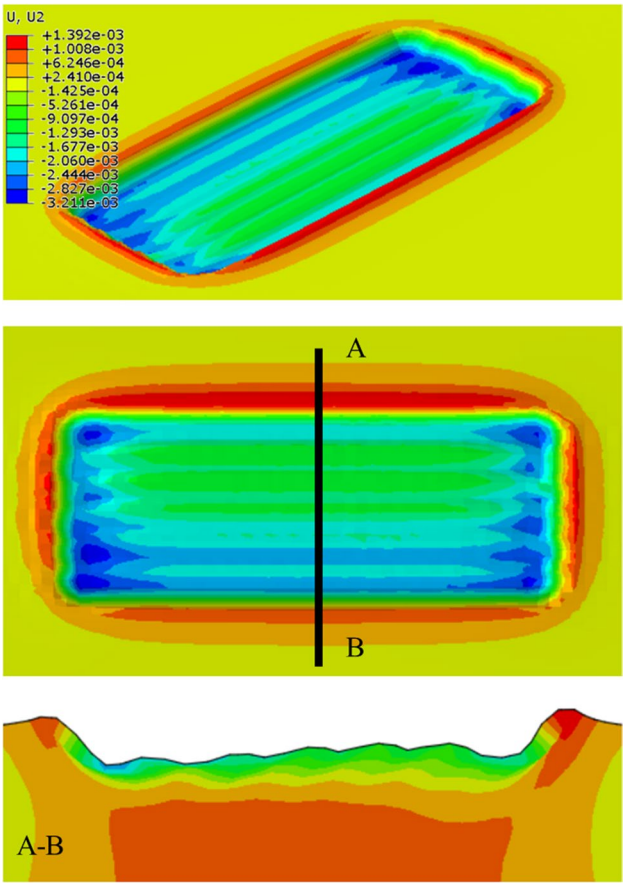

Fig. 13 Displacement cloud map of micro-textures fabricated by USRP

shows that regular, flat, and periodically distributed micro-groove arrays are fabricated on the steel substrate surface by USRP treatment. And the processed surface micro-textures have high processing accuracy. The topography on the A-B cross-section shows that the micro-groove arrays are relatively uniformly distributed in depth. The micro-texture arrays consist of a periodic staggered arrangement of micro-grooves and micro-bulges, which is due to the fact that USRP treatment is an iso-material process and the plastic flow characteristics of the material lead to the formation of bulge structures around the micro-grooves.

Figure 14 shows the stress simulation contour of the micro-textured surface layer under the above USRP parameters. From Fig. 14(a), it can be found that a stable plastic deformation zone with relatively uniform stress distribution is formed in the textured processing area. And an impact-affected zone with high local stress is produced due to the continuous accumulation of stress in the last pass of machining micro-grooves. Moreover, the stress state induced by the micro-textured surface layer is a high value of residual compressive stress, which indicates that the USRP texturing process achieves the stress strengthening of the substrate. The residual stress distribution along the depth direction can be divided into three regions (Fig. 14(b)), including the I, II, and III regions. I region is the residual compressive stress region in the outermost layer, II region is the residual tensile stress layer, and III region is the residual tensile stress layer inside the base material. The residual compressive stress in I region is favorable to retard the initiation and propagation of micro-cracks on the machined surface. Instead, the

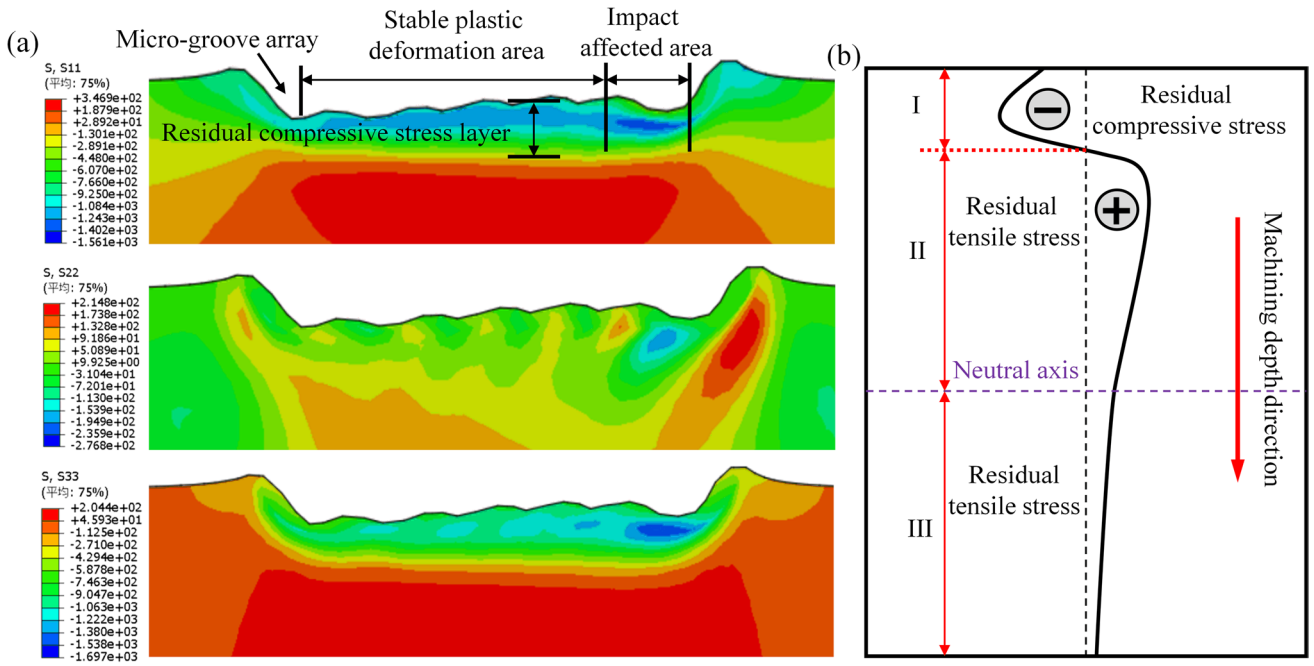

Fig. 14 The stress distribution of the micro-textures machined by USRP along the depth direction

residual tensile stress state in II region increases the crack growth rate. The residual tensile stress in III region is so small that its influence can be ignored. Hence, the micro-textured surface with the high-value residual compressive stress machined by USRP is beneficial to improving the serviceability and fatigue life of the material surface.

After USRP texturing, the textured surface layer undergoes work hardening, which is manifested by a significant increase in hardness. The degree of work hardening of the material can be characterized by the amount of plastic deformation. To reflect the accumulation process of plastic deformation, the equivalent plastic strain (PEEQ) can be chosen to characterize the work hardening effect of the material after USRP texturing treatment. Figure 15 shows the distribution of the PEEQ along the micro-texture depth direction under the same texturing parameters as mentioned above. It can be seen that a layer of strain strengthening area with significantly increased PEEQ appears in the micro-textured region, which indicates that the USRP enables the textured surface layer to achieve strain strengthening.

The energy changes during USRP texturing can reveal the interaction between the ultrasonic rolling ball and the material surface, in addition to reflecting the texturing effect. In general, the energy generated in the mechanical process includes artificial strain energy, creep dissipation energy, damage dissipation energy, external work, frictional dissipation, internal energy, kinetic energy, plastic dissipation, strain energy, total energy, and viscous dissipation [27, 28]. Figure 16 shows the variation of each component of the generated energy during single-pass micro-groove machining with a static pressure of 300 N, an amplitude of 7 mm, and a feed speed of 1000 mm/min. For the whole model, the variation of energy shows a significant difference in the three analysis step stages. During the first analysis step (within 0–0.05 s), the initial contact of the rolling ball with the machined surface occurs, and the individual component of the total energy begins to vary and fluctuate. During the stable texturing stage (0.05–0.25 s), artificial strain energy, creep dissipation energy, damage dissipation energy, and viscous dissipation are approximately 0. At this stage, the work is mainly done by the external loads generated by static pressure and dynamic impact force, which can be observed from the gradual increase of the external work in Fig. 16(b). Moreover, the internal energy, plastic dissipation, and strain energy all show an overall increase accompanied by fluctuations, which indicates that the USRP texturing was a process of continuous plastic deformation and further proved the strain hardening phenomenon of the micro-textured surface. The internal energy of the system consists of plastic dissipation, strain energy, creep dissipation energy, and artificial strain energy. Since artificial strain energy and creep dissipation energy are almost 0, the internal energy is superimposed by plastic dissipation and strain energy. It can be seen that at 0.25 s, the internal energy is ~ 7.0 mJ, the strain energy is ~ 1.5 mJ, and the plastic dissipation is ~ 6.0 mJ. After the rolling ball is lifted off the machined surface (0.25–0.3 s), the kinetic energy first increases to a maximum value and then decreases to 0. The internal energy, plastic dissipation,

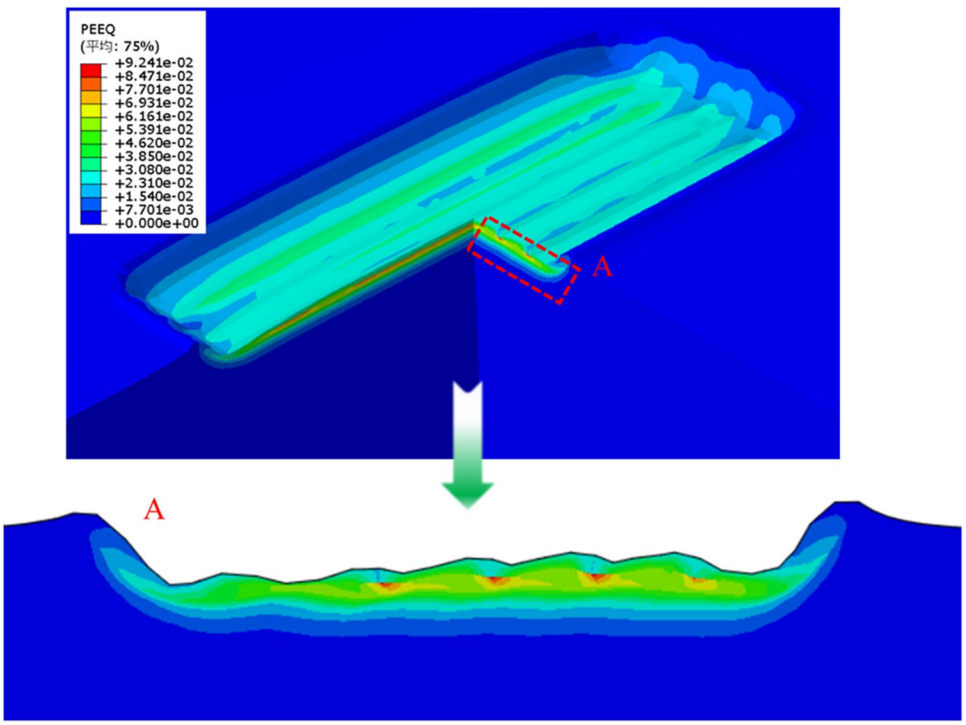

Fig. 15 The PEEQ distribution of the micro-textured surface after USRP texturing

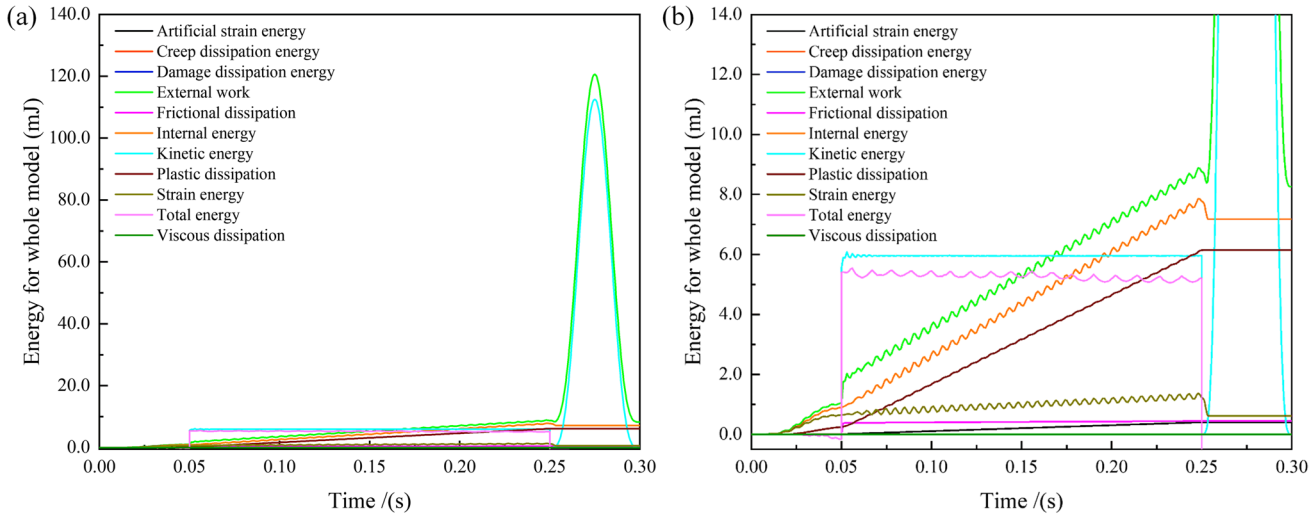

Fig. 16 Energy variety during USRP texturing process

and strain energy are all stable at positive values and slightly lower than the maximum value generated during the stable texturing process, indicating that the material undergoes partial elastic recovery and a small amount of strain energy is released. However, most of the strain energy remains stored at the surface, causing permanent plastic deformation to form micro-textured topography.

4 Experimental validation

To demonstrate the accuracy of the analytical model and FEM model describing the USRP texturing process, the calculated and simulated depth values of micro-grooves were compared with the experimental results, respectively. The USRP texturing test is conducted on a USRP device assembled on the vertical machining center DAEWOO ACE-V500. The substrate to be micro-textured is AISI 5140 steel with a size of $15 \times 15 \times 5$ mm^3. A YG6 ball with a diameter of 6 mm is used as an ultrasonic rolling head. During USRP texturing, ultrasonic vibration is applied to the rolling ball along the machine spindle in the *Z*-direction, and the machined steel sample is fixed on the table. The rolling ball is fed in an *S*-shaped path in the *X* and *Y* directions concerning the textured sample, as depicted in Fig. 17. The basic machining parameters of the USRP texturing process are listed in Table 4.

After USRP texturing, the surface topographies of micro-textures are observed by a white light interferometer (Wyko NT9300, Veeco Inc., USA). The micro-hardness *H* is acquired by a nano-indenter (HM2000S, Helmut Fischer, Germany) with the maximum applied load of 30 mN. For each sample, three measurements are taken to ensure the reliability of the data obtained.

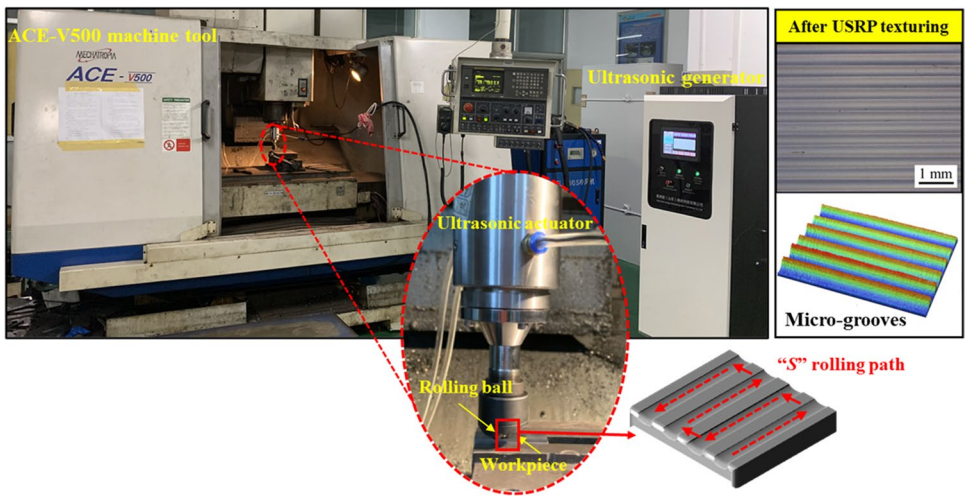

Fig. 17 USRP texturing experiment for AISI 5140 steel substrate

Table 4 The basic parameters of the USRP texturing process

Basic parameters	Values
Frequency (kHz)	28
Amplitude (μm)	7
Static pressure (N)	300–900
Feed speed (mm/min)	1000
Step distance (μm)	50–300

The micro-groove morphology based on the FEM model is first obtained and compared with the experimental results under the same processing parameters, as shown in Fig. 18. The simulated and experimental texturing is performed with an amplitude of 7 μm, a static pressure of 300 N, and a feed speed of 1000 mm/s. Besides, the simulated data and experimental results of the cross-sectional profile of a single micro-groove are compared under static pressure of 300 N, 450 N, and 600 N, and the comparative results are presented in Fig. 19. The surface morphology and dimension of the micro-grooves obtained by the FEM model are basically consistent with the results obtained from experimental processing, which proves that the established FEM model for the single-pass USRP texturing process is accurate and reliable.

The micro-groove array is then simulated by the multi-pass FEM model of the USRP texturing process with the same texturing parameters as in Fig. 18. The step distance is 300 μm. The comparison result with the experimental morphology is shown in Fig. 20. As shown in Fig. 20, the simulated morphology of the micro-textures is in good agreement with the experimental results. The spacing of adjacent micro-textures is 300 μm, which is consistent with the set step distance. The micro-grooves all show a uniform and regular arrangement. Figure 21 shows the simulated and experimental cross-sectional profile of the micro-groove array fabricated by USRP depicted in Fig. 20. It can be seen that the simulated micro-groove array has a regular profile with uniform depth variation. In contrast, the experimentally obtained depths between adjacent microgrooves are

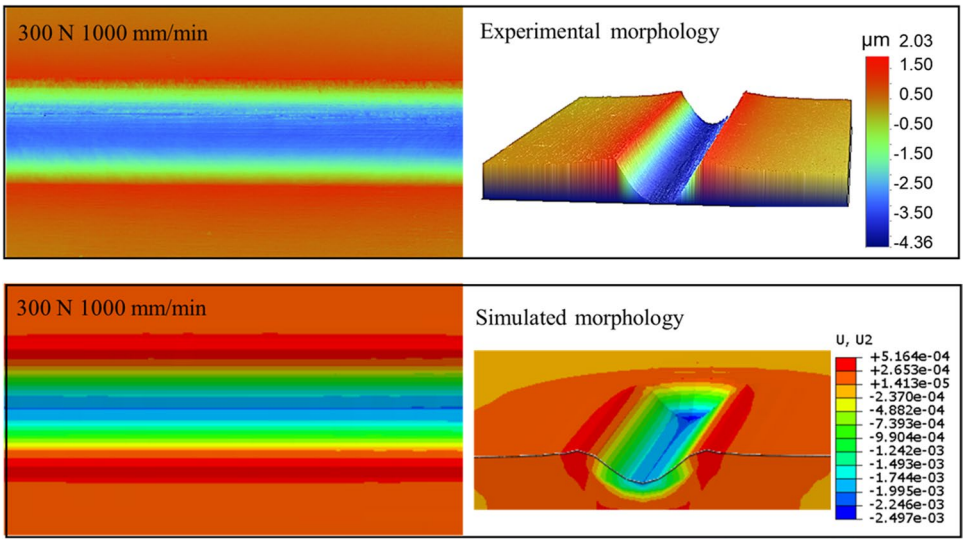

Fig. 18 Simulated and experimental topographies of single micro-groove fabricated by USRP

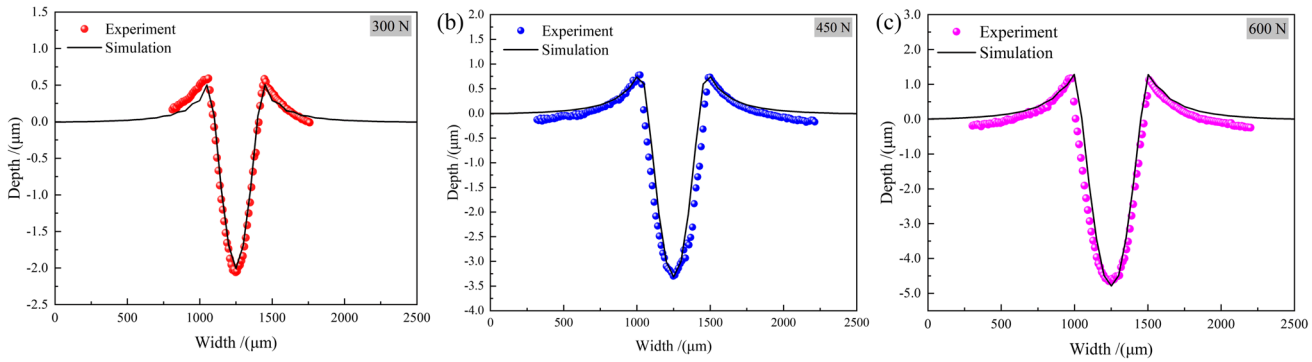

Fig. 19 Simulation and experimental dimensions of single micro-groove fabricated by USRP

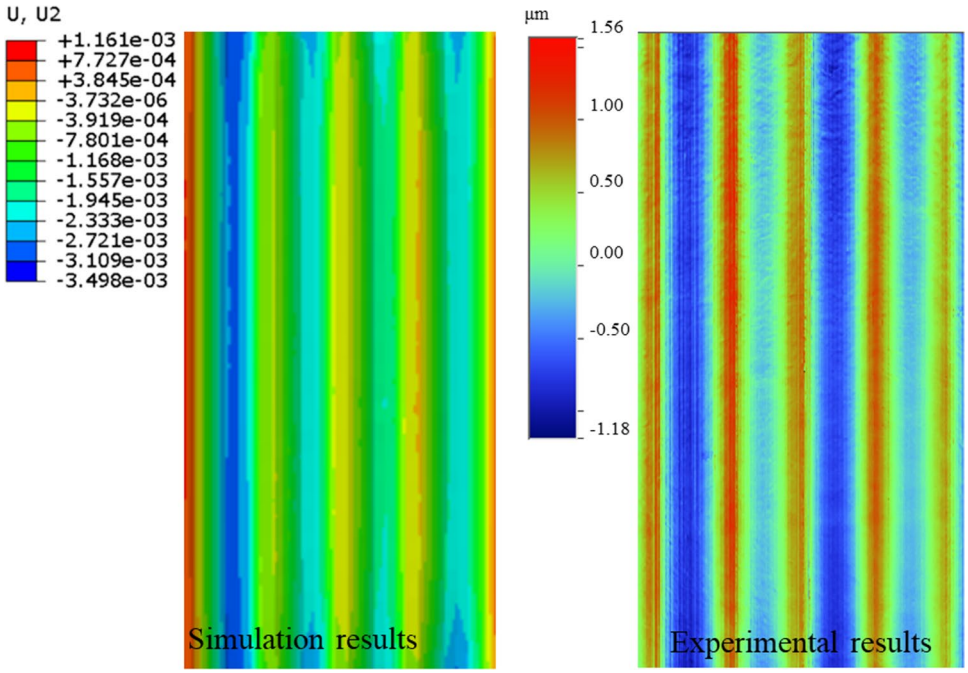

Fig. 20 Simulated and experimental surface topography of multi-pass micro-grooves fabricated by USRP at the step distance of 300 μm

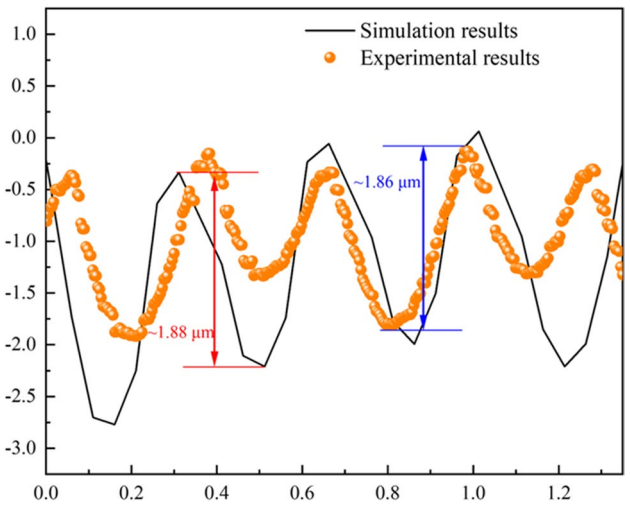

Fig. 21 Comparison of the simulated and experimental profile of multi-pass micro-grooves fabricated by USRP at the step distance of 300 μm

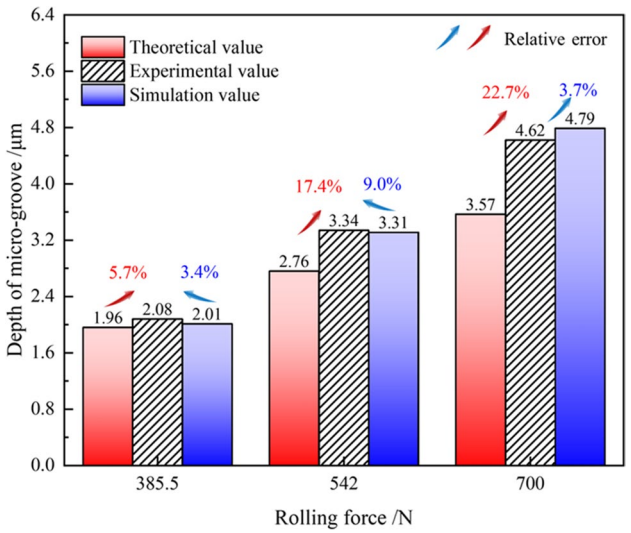

Fig. 22 Comparison results and relative errors of the micro-groove depth obtained from the analytical model, FEM prediction, and experimental machining

less uniform, which is influenced by the formation of micro-bulge structure and the mutual restraint of plastic flow of materials in adjacent passes. The errors in Fig. 21 are caused by the differences between the actual plasticity behavior and the theoretical plasticity model of AISI 5140 steel. Overall, these errors are acceptable and the FEM model for the multi-pass USRP texturing process is reliable.

Finally, the consistency of the results between the analytical model, the FEM model, and the experimental machining is judged. The average micro-hardness H of polished AISI 5140 steel surface is 7.44 GPa. As a result, the theoretical result of the micro-groove height is calculated according to Eq. (20). The comparison results and relative errors of the calculated data, FEM result, and the experimental value of the micro-groove height are summarized in Fig. 22. When the rolling forces were 385.5 N, 542 N, and 700 N, compared with experimental values, the theoretical model showed a relative error of 5.7%, 17.4%, and 22.7%, respectively, and the FEM model showed the relative error of 3.4%, 9.0%, and 3.7%, respectively. Accordingly, the established FEM model is feasible and accurate to predict the USRP texturing

process, and further revisions to the theoretical model may be required for accurately predicting the micro-textured dimension under high rolling force processing.

5 Conclusions

In this study, the theoretical model and FEM model of the micro-texture formation mechanisms based on USRP texturing were established. The main contributions are as follows:

(1) Focusing on the elastic–plastic deformation behavior of USRP combined with the micro-structure strengthening mechanism, the feasibility of fabricating micro-textures by USRP was analyzed, and the effective gain of USRP texturing was summarized.
(2) The theoretical model was deduced to describe the geometrical relationship of the contact regions forming the micro-textures during USRP texturing, and the geometric controllability of the fabricated micro-textures was discussed. The dimension parameters of micro-grooves were closely related to USRP machining parameters, including amplitude, frequency, static pressure, machining step, and feed speed. The relationship between micro-texture depth and USRP machining parameters, which is proportional to the rolling force, was quantitatively evaluated.
(3) Based on the ultrasonic single-point impact FEM model, the dynamic response of the rolling head was analyzed and the effect of USRP machining parameters on the micro-texture size was predicted. The further developed multi-pass USRP texturing FEM model revealed the generation mechanism and enhanced mechanical response characteristics of micro-textures from the stress, strain, and energy perspectives. The theoretical and FEM models were examined and compared with the experimental micro-texture characterization, showing good agreement.
(4) Through analytical, simulation, and experimental analysis, USRP is demonstrated to be a potential surface texturing method capable of producing micro-texture arrays with high accuracy and efficiency. The overall results indicate that the proposed models can serve as a useful approach for predicting the micro-texture fabricating process and designing appropriate texturing process parameters.

Author contribution All authors contributed to the study conception and design. Methodology, data curation, conceptualization, and writing-original draft preparation were performed by Ying Meng and Jianxin Deng. Supervision, writing-reviewing, supervision, and validation were performed by Ran Wang, Qinghao Sun, and Zhihui Zhang. All authors read and approved the final manuscript.

Funding This work is supported by the National Natural Science Foundation of China (52275443) and the Key Research and Development Projects of Shandong Province (2020CXGC011003).

Declarations

Competing interests The authors declare no competing interests.

References

1. Chen HW, Zhang LW, Zhang DY, Zhang PF, Han ZW (2015) Bioinspired surface for surgical graspers based on the strong wet friction of tree frog toe pads. ACS Appl Mater Inter 7(25):13987–13995. https://doi.org/10.1021/acsami.5b03039
2. Chen YP, Meng JX, Gu Z, Wan XZ, Jiang LM, Wang ST (2020) Bioinspired multiscale wet adhesive surfaces: structures and controlled adhesion. Adv Funct Mater 30(5):1905287. https://doi.org/10.1002/adfm.201905287
3. Liu WL, Ni HJ, Wang P, Chen HL (2020) Investigation on the tribological performance of micro-dimples textured surface combined with longitudinal or transverse vibration under hydrodynamic lubrication. Int J Mech Sci 174:105474. https://doi.org/10.1016/j.ijmecsci.2020.105474
4. Salguero J, Del Sol I, Vazquez-Martinez JM, Schertzer MJ, Iglesias P (2019) Effect of laser parameters on the tribological behavior of Ti6Al4V titanium microtextures under lubricated conditions. Wear 426–427:1272–1279. https://doi.org/10.1016/j.wear.2018.12.029
5. Lu P, Wood R (2020) Tribological performance of surface texturing in mechanical applications-a review. Surf Topogr-Metrol 8(4):043001. https://doi.org/10.1088/2051-672x/abb6d0
6. Guo ZW, Huang QR, Xie X, Yuan CQ (2021) Effects of spherical-platform texture parameters on the tribological performance of water-lubricated bearings. Wear 477:203863. https://doi.org/10.1016/j.wear.2021.203863
7. Pratap T, Patra K (2020) Tribological performances of symmetrically micro-textured Ti-6Al-4V alloy for hip joint. Int J Mech Sci 182:105736. https://doi.org/10.1016/j.ijmecsci.2020.105736
8. Vidyasagar KEC, Pandey RK, Kalyanasundaram D (2021) An exploration of frictional and vibrational behaviors of textured deep groove ball bearing in the vicinity of requisite minimum load. Friction 9:1749–1765. https://doi.org/10.1007/s40544-021-0495-3
9. Kang ZY, Fu YH, Zhou DS, Wu QQ, Chen TY, He YY, Su XP (2021) Reducing engine oil and fuel consumptions by multidimensional laser surface texturing on cylinder surface. J Manuf Process 64:684–693. https://doi.org/10.1016/j.jmapro.2021.01.052
10. Pang K, Wang DZ (2020) Study on the performances of the drilling process of nickel-based superalloy Inconel 718 with differently micro-textured drilling tools. Int J Mech Sci 180:105658. https://doi.org/10.1016/j.ijmecsci.2020.105658
11. Kawasegi N, Ozaki K, Morita N, Nishimura K, Yamaguchi M (2017) Development and machining performance of a textured diamond cutting tool fabricated with a focused ion beam and heat treatment. Prec Eng 47:311–320. https://doi.org/10.1016/j.precisioneng.2016.09.005
12. Shimizu J, Nakayama T, Watanabe K, Yamamoto T, Onuki T, Ojima H, Zhou LB (2020) Friction characteristics of mechanically microtextured metal surface in dry sliding. Tribol Int 149:105634. https://doi.org/10.1016/j.triboint.2019.02.042

13. Li KM, Yao ZQ, Hu YX, Gu WB (2014) Friction and wear performance of laser peen textured surface under starved lubrication. Tribol Int 77:97–105. https://doi.org/10.1016/j.triboint.2014.04.017
14. Zhou MH, Xu YH, Liu Y et al (2021) Microstructures and mechanical properties of Mg-15Gd-1Zn-0.4Zr alloys treated by ultrasonic surface rolling process. Mater Sci Eng A 828:141881. https://doi.org/10.1016/j.msea.2021.141881
15. Karademir I, Celik MB, Husem F, Maleki E, Amanov A, Unal O (2021) Effects of constrained groove pressing, severe shot peening and ultrasonic nanocrystal surface modification on microstructure and mechanical behavior of S500MC high strength low alloy automotive steel. Appl Surf Sci 538:147935. https://doi.org/10.1016/j.apsusc.2020.147935
16. Wang BY, Yin Y, Gao ZW, Hou ZB, Jiang WC (2017) Influence of the ultrasonic surface rolling process on stress corrosion cracking susceptibility of high strength pipeline steel in neutral pH environment. RSC Adv 7:36876–36885. https://doi.org/10.1039/c7ra05425d
17. Kheradmandfard M, Kashani-Bozorg SF, Kim C-L, Hanzaki AZ, Pyoun YS, Kim J-H, Amanov A, Kim D-E (2017) Nanostructured beta-type titanium alloy fabricated by ultrasonic nanocrystal surface modification. Ultrason Sonochem 39:698–706. https://doi.org/10.1016/j.ultsonch.2017.03.061
18. Evseev DG, Medvedev BM, Grigoriyan GG (1991) Modification of the elastic-plastic model for the contact of rough surfaces. Wear 150(1–2):79–88. https://doi.org/10.1016/0043-1648(91)90307-g
19. Johnson KL (1985) Contact mechanics. Cambridge University Press, Cambridge
20. Zhao J, Wang B, Liu ZQ (2016) The Investigation into burnishing force, burnishing depth and surface morphology in rotary ultrasonic burnishing. Acta Armamentarii 37:9. https://doi.org/10.3969/j.issn.1000-1093.2016.04.018
21. Wu Z, Bao H, Xing YQ, Liu L (2022) Heat transfer performance and prediction of open pulsating heat pipe for self-cooling cutting tool. Int J Adv Manuf Tech 121:6951–6972. https://doi.org/10.1007/s00170-022-09796-8
22. Mariangela Q, Gianluca D, Claudio G, Giancarlo M (2020) FEM model development for the simulation of a micro-drilling EDM process. Int J Adv Manuf Tech 1060:3095–3104. https://doi.org/10.1007/s00170-019-04750-7
23. Tomasz T, Francesco D, Hirpa GL (2021) Multiphysics modeling and numerical simulation in computer-aided manufacturing processes. Metals 11(1):175. https://doi.org/10.3390/met11010175
24. Jiang T, Zhou W, Tang J, Zhao X, Zhao J, Liu H (2022) Constitutive modelling of AISI 9310 alloy steel and numerical calculation of residual stress after shot peening. Int J Impact Eng 166:104235. https://doi.org/10.1016/j.ijimpeng.2022.104235
25. Wang F, Men XH, Liu YJ, Fu XL (2020) Experiment and simulation study on influence of ultrasonic rolling parameters on residual stress of Ti-6Al-4V alloy. Simul Model Pract Th 104:102121. https://doi.org/10.1016/j.simpat.2020.102121
26. Liu Y, Wang LJ, Wang DP (2011) Finite element modeling of ultrasonic surface rolling process. J Mater Process Tech 211(12):2106–2113. https://doi.org/10.1016/j.jmatprotec.2011.07.009
27. Eom TS, Park HG (2010) Evaluation of energy dissipation of slender reinforced concrete members and its applications. Eng Struct 32(9):2884–2893. https://doi.org/10.1016/j.engstruct.2010.05.007
28. Honig A, Stronge WJ (2000) Dynamic buckling of an imperfect elastic, visco-plastic plate. Int J Impact Eng 24(9):907–923. https://doi.org/10.1016/s0734-743x(00)00007-5